31. Addition of 1 weight % core material to a mantle source will have no effect on the isotopes of Sr, Nd, Pb, and oxygen, which are well correlated with Os isotopes in most OIBs [for example, Hawaii (*18*, *19*)]. Core-mantle interaction would also buffer the f_{O_2} of OIBs to the iron-wustite buffer, which is three to four orders of magnitude lower than f_{O_2}'s actually measured in OIBs [*Basaltic Volcanism Study Project* (Pergamon Press, New York, 1981)].
32. K. Righter, M. J. Drake, G. Yaxley, *Phys. Earth Planet. Int.* **100**, 115 (1997).
33. J. Myers and H. Eugster, *Contrib. Mineral. Petrol.* **82**, 75 (1983).
34. T. Meisel, R. J. Walker, J. W. Morgan, *Nature* **383**, 517 (1996); H. K. Brueckner *et al.*, *J. Geophys. Res.* **100**, 22283 (1995); L. Reisberg and J.-P. Lorand, *Nature* **376**, 159 (1995); J. W. Morgan, G. A. Wandless, R. K. Petrie, A. J. Irving, *Tectonophysics* **75**, 47 (1981).
35. T. H. Green, *Chem. Geol.* **117**, 1 (1994).
36. We thank C. J. Capobianco, J. Chesley, M. J. Drake, S. Shirey, and P. Warren for discussions; P. Liermann and J. Ganguly for providing samples of Buell Park garnet; and J. Wang for expert assistance with the ion microprobe. This research is supported by NSF grants EAR-9706024 and EAR-9628092.

24 March 1998; accepted 29 April 1998

Integrated Optoelectronic Devices Based on Conjugated Polymers

Henning Sirringhaus,* Nir Tessler, Richard H. Friend*

An all-polymer semiconductor integrated device is demonstrated with a high-mobility conjugated polymer field-effect transistor (FET) driving a polymer light-emitting diode (LED) of similar size. The FET uses regioregular poly(hexylthiophene). Its performance approaches that of inorganic amorphous silicon FETs, with field-effect mobilities of 0.05 to 0.1 square centimeters per volt second and ON-OFF current ratios of $>10^6$. The high mobility is attributed to the formation of extended polaron states as a result of local self-organization, in contrast to the variable-range hopping of self-localized polarons found in more disordered polymers. The FET-LED device represents a step toward all-polymer optoelectronic integrated circuits such as active-matrix polymer LED displays.

Solution-processible conjugated polymers are among the most promising candidates for a cheap electronic and optoelectronic technology on plastic substrates. Polymer LEDs exceeding peak brightnesses of 10^6 cd m^{-2} (*1*) and high-resolution video polymer LED displays (*2*) have been demonstrated. One of the main obstacles to all-polymer optoelectronic circuits is the lack of a polymer FET with sufficiently high mobility and ON-OFF ratio to achieve reasonable switching speeds in logic circuits (*3*) and to drive polymer LEDs.

Conjugated polymer FETs (*4*) typically show field-effect mobilities of $\mu_{FET} = 10^{-6}$ to 10^{-4} cm^2 V^{-1} s^{-1}, limited by variable-range hopping between disordered polymer chains and ON-OFF current ratios of $<10^4$ (*5*). This is much too low for logic and display applications, and therefore all previous approaches to drive polymer LEDs have used polycrystalline (*2*) or amorphous silicon (a-Si) (*6*) technology. Recently, a polymer FET with a mobility of 0.01 to 0.04 cm^2 V^{-1} s^{-1} and an ON-OFF ratio of 10^2 to 10^4 using regioregular poly(hexylthiophene) (P3HT) was described (*7*). The high mobility is related to structural order in the polymer film induced by the regioregular head-to-tail (HT) coupling of the hexyl side chains. However, a clear understanding of the transport mechanism giving rise to the relatively high mobilities is still lacking.

Here, we report a considerably improved P3HT FET reaching mobilities of 0.05 to 0.1 cm^2 V^{-1} s^{-1} and ON-OFF ratios of $>10^6$, the performance of which starts to rival that of inorganic a-Si FETs and enables us to demonstrate integrated optoelectronic polymer devices. As an example, we have chosen a simple pixel-like configuration in which the FET supplies the current to a polymer LED. This allows us to assess the prospects of active-matrix addressing in all-polymer LED displays.

To construct the multilayer device (Fig. 1A), we first fabricated the FET by spin-coating a film of P3HT (500 to 700 Å) (*8*) onto a highly doped n^+-Si wafer with a 2300 Å SiO_2 gate oxide (capacitance $C_i = 15$ nF cm^{-2}). Au source-drain contacts were deposited onto the P3HT through a shadow mask. Then, a layer of SiO_x was thermally evaporated through another, mechanically aligned, shadow mask to define the active LED area on the finger-shaped Au FET drain electrode acting as the hole-injecting anode of the LED. A single layer of poly[2-methoxy-5-(2′-ethyl-hexyloxy)-*p*-phenylenevinylene] (MEH-PPV) was spin-coated on top. Evaporation of a semitransparent Ca-Ag cathode completed the device. No photolithographic steps were involved. The device

Cavendish Laboratory, University of Cambridge, Madingley Road, Cambridge CB3 0HE, UK.
*To whom correspondence should be addressed.

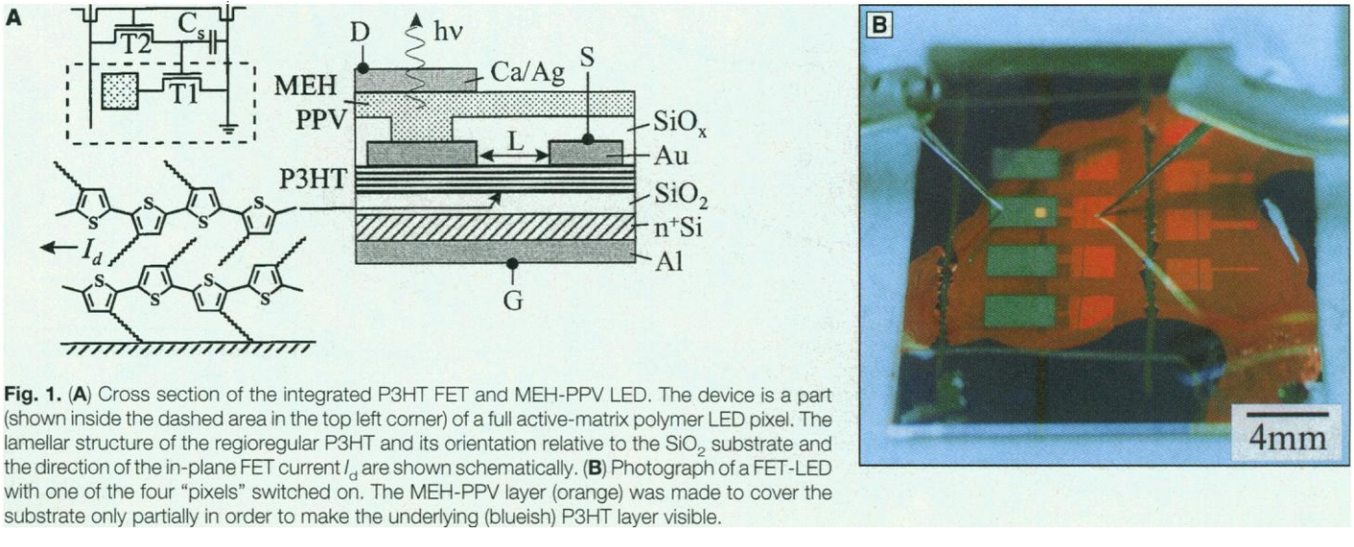

Fig. 1. (**A**) Cross section of the integrated P3HT FET and MEH-PPV LED. The device is a part (shown inside the dashed area in the top left corner) of a full active-matrix polymer LED pixel. The lamellar structure of the regioregular P3HT and its orientation relative to the SiO_2 substrate and the direction of the in-plane FET current I_d are shown schematically. (**B**) Photograph of a FET-LED with one of the four "pixels" switched on. The MEH-PPV layer (orange) was made to cover the substrate only partially in order to make the underlying (blueish) P3HT layer visible.

is a part of an active-matrix LED display pixel (9), which would require an additional transistor T2 and a storage capacitor C_s controlling the voltage on the gate of T1 (Fig. 1A).

When the FET was switched on (Fig. 1B), the current flowed from the FET source electrode (right contact probe) to the LED cathode (left contact probe). Evidently, the LED could be switched on and off by the FET gate voltage V_g (Fig. 2A). At $V_g = -50$ V, the FET supplied a current density of ~10 mA cm^{-2} to the LED, resulting in a brightness on the order of 1 cd m^{-2}. From the linear relation between the FET current I_d and the detected photocurrent I_p (Fig. 2B), we estimate the external LED quantum efficiency to be $\eta_{ext} \approx 0.01\%$. This value is much smaller than in an optimized MEH-PPV LED with $\eta_{ext} = 1\%$ (*10*). This is attributed to nonoptimized carrier injection at the Au and Ca-Ag electrodes, the use of a single-layer LED, and absorption losses in the 20-nm Ca-Ag cathode. With an optimized LED ($\eta_{ext} > 1\%$) (*10*), the current density of 10 mA cm^{-2} supplied by the FET, which is regarded as a design rule for polymer LED displays, should be sufficient to achieve a practical video brightness of 100 cd m^{-2}. If the channel length L were reduced from 75 μm to ~20 μm, the width W of the FET could be scaled down to integrate the device fully along one edge (with length d) of the LED anode—that is, $W \approx d$—such that it occupies only a small area.

Our simple device does not address the complex issues of integrating a full pixel structure (9), which would also require the use of polymeric insulators (*11*). Moreover, to lower the high FET operating voltage, it is necessary to reduce the gate insulator thickness and to improve the subthreshold characteristics (see below). However, the device clearly demonstrates that high-mobility P3HT FETs have sufficient driving current to switch polymer LEDs of similar size ($W \approx d$). The relative crudeness of our integration scheme illustrates the ease of fabrication and the robustness of solution-processed conjugated polymers for multilayer integrated devices. (Our first attempts to realize the FET-LED with an oligomer FET deposited by vacuum sublimation failed, as the buried FETs degraded during the deposition of subsequent layers. No degradation was observed for P3HT devices.)

In the following, we focus on the improvement and transport mechanism of the P3HT transistors as the key element of the integrated device. A typical improved P3HT FET switches on sharply around $V_0 = 0$ to 4 V, with good subthreshold slopes of 1 to 1.5 V decade^{-1} (Fig. 3A). The ON-OFF ratio between $V_g \approx 0$ V and $V_g = -60$ V exceeds 10^6, the OFF current being limited by gate leakage. The film conductivity σ is $<10^{-8}$ S cm^{-1}. From the transfer characteristics in the saturation regime, we extract mobilities $\mu_{FET} = 0.05$ to 0.1 cm^2 V^{-1} s^{-1}, depending on the details of device preparation. This improvement of the ON-OFF ratio by two orders of magnitude and of the mobility by a factor of 2 (*7*) is attributed to the optimized device fabrication reducing unintentional doping and promoting self-organization of the polymer. All solution preparation and device processing steps were performed in a dry N_2 atmosphere, because the conductivity of P3HT films was found to increase upon exposure to air for a few minutes. Deposition of a layer of SiO_x (Fig. 1A) onto the surface of such air-exposed films restored the low conductivity, which suggests that the substoichiometric SiO_x attracts dopants from the P3HT surface layer. From capacitance-voltage measurements on n^+-Si–SiO_2–P3HT–Au diodes, we estimate the residual bulk doping level of carefully processed P3HT films to be ~5×10^{15} cm^{-3}. The mobility increase is partly attributed to predeposition treatment of the Si-SiO_2 substrate with the silylating agent hexamethyldisilazane replacing the natural hydroxyl groups on the SiO_2 surface with apolar methyl groups. Although the atomic interface structure is not known, this is believed to promote phase segregation of the polymer at the interface (Fig. 1A). The deposition onto a flat surface was also found to be advantageous relative to coating the polymer onto a substrate with prefabricated source-drain contacts (*7*). Films were spin-coated at 2000 rpm from a solution of P3HT (0.7 to 0.8 weight %) in $CHCl_3$.

Regioregular P3HT with $\mu_{FET} \approx 0.1$ cm^2 V^{-1} s^{-1} and $\sigma < 10^{-8}$ S cm^{-1} clearly does not follow the "universal relationship" between conductivity and mobility ($\mu_{FET} \propto \sigma^{\delta}$, $\delta \approx 0.7$) that is characteristic of variable-range hopping in more disordered conjugated polymers (*5*). The mobility is of the same order of magnitude as in polycrystalline oligomer FETs with related structures such as α-sexithiophene (*11*) and approaches the mobility of molecular single-crystal FETs (~1 cm^2 V^{-1} s^{-1}) (*12*). This strongly suggests that the origin of the exceptionally high polymer mobilities reported here is the formation of extended current-transporting states similar to those in structurally related oligomers. Extended states cannot be formed unless there is at least short-range, if not microcrystalline, order. X-ray diffraction shows that on a local scale, regioregular P3HT has a lamellar, phase-segregated structure with alternating layers of conjugated backbones and interdigitated side chains parallel to the substrate (*7*, *13*), favorable for in-plane FET transport (Fig. 1A) (*14*). Extended-state formation is believed to be the result of relatively long conjugation lengths along polymer chains (*8*) and π-π stacking of adjacent chains. Grain boundaries between the small crystalline domains with more disordered chain conformation, residual doping, and other structural or chemical defects give rise to localized trap states.

This electronic structure justifies the analysis of the FET characteristics in terms of a model that has proven very successful for a-Si FETs (*15*) and has already been applied to oligomer FETs (*12*, *16*). The model assumes that the current is transported by extended (that is, high-mobility) states above a

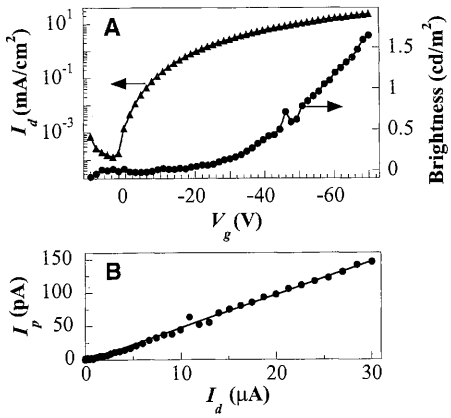

Fig. 2. (**A**) Brightness of the LED (circles) and drain current I_d supplied by the FET to the LED (triangles) as a function of the FET gate voltage V_g. I_d is normalized by the area A of the LED. (**B**) Linear relationship between I_d and the photocurrent I_p detected by a Si photodiode above the LED (A = 300 μm by 430 μm, channel length L = 75 μm, channel width W = 1500 μm, source-drain voltage $V_{sd} = -70$ V).

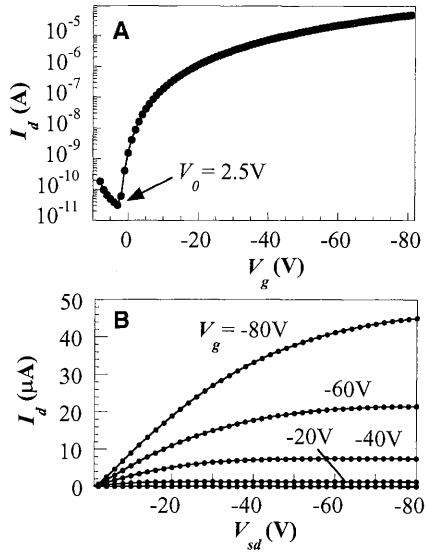

Fig. 3. (**A**) Transfer characteristics in the saturation regime ($V_{sd} = -80$ V) and (**B**) output characteristics of a typical P3HT FET (L = 75 μm, W = 1500 μm).

mobility edge E_c, below which there is a tail of localized states with much lower mobility, but it makes no further assumptions about the nature of the localized states, nor about the transport mechanism above E_c. Hence, the model may also be applicable to polarons in a conjugated polymer. The transconductance dI_d/dV_g in the saturation regime is given by

$$\frac{dI_d}{dV_g} = e\frac{W}{L}\mu_{FET}(n^s_{ind})\, n^s_{ind}(V_g) \qquad (1)$$

(*15*), where the field-effect mobility μ_{FET} is defined by

$$\mu_{FET}(n_{ind}, T) = \mu_0(T)\frac{n_f}{n_{ind}}(T) \qquad (2)$$

and where n_{ind} (n^S_{ind}) is the total density of induced interface carriers with elementary charge e [at the source (S) electrode], and n_f is the fraction of n_{ind} in current-transporting states above E_c with mobility μ_0. Neglecting the small variation of the Fermi level E_F with V_g, n^S_{ind} increases linearly with V_g, that is, $n^S_{ind} \approx C_i/e(V_g - V_{FB})$ above the flat-band voltage V_{FB}.

If the tail of localized trap states is steep, E_F is below the typical tail state energy E_t and varies little with V_g. Then, $\mu_{FET} \propto \mu_0 \exp[-(E_c - E_t)/kT]$ is constant, resulting in a linear dependence of dI_d/dV_g on $(V_g - V_T)$ above the threshold voltage V_T. This is observed in high-quality a-Si (*17*) and in most oligomer FETs. However, if E_F enters the distribution of localized states, for example, for a relatively broad distribution, μ_{FET} exhibits a strong dependence on n_{ind}. This seems to be the case in P3HT FETs.

Around room temperature, the transconductance of a typical P3HT FET is linear above $|V_g| > 30$ V ($|V_T| = 10$ to 20 V), corresponding to a constant field-effect mobility of $\mu_{FET} = 0.05$ to 0.1 cm^2 V^{-1} s^{-1} (Fig. 4A). However, there is an extended nonlinear region between the transistor switch-on at V_0 and V_T in which μ_{FET} depends on V_g. At low temperatures, μ_{FET} depends on V_g in the whole observable voltage range (*18*). At fixed values of n^S_{ind}, the mobility calculated from Eq. 1 (*19*) shows a roughly exponential temperature dependence proportional to $\exp(-E_a/kT)$ with positive deviations below ~150 K (Fig. 4B). Below ~80 K, measurements were not possible because of increased turn-on voltages indicating disorder-induced carrier localization. The activation energies $E_a = 60$ to 100 meV are similar to those of oligomer and a-Si FETs (*17*) but are small relative to hopping activation energies in low-mobility polymers ($E_a > 0.2$ eV) (*5*). The decrease of E_a with increasing n^S_{ind} (Fig. 4C) suggests that the dominant exponential temperature variation of μ_{FET} reflects the distribution of localized states—that is, the ratio $n_f/n_{ind}(T)$ (see Eq. 2)—and not a possible temperature dependence of $\mu_0(T)$, which is not expected to depend on n_{ind}.

We do not attempt here to deduce information about the distribution of localized states, which would require careful device modeling and independent spectroscopic measurements. Therefore, an estimate of the magnitude of the trap-free mobility μ_0 and the corresponding mean free path length cannot be given at present. [For a-Si with $\mu_{FET} = 0.1$ to 1 cm^2 V^{-1} s^{-1}, $\mu_0 \approx 10$ cm^2 V^{-1} s^{-1} has been estimated (*17*).] We can conclude, however, that our model involving extended polaron states induced by local self-organization and disorder-induced localized states allows a consistent understanding of the exceptionally high room-temperature mobilities (close to those of oligomers with much higher polycrystalline order) and of the thermally activated temperature dependence. The latter mainly reflects the distribution of localized states rather than any intrinsic properties of polaron hopping (*20*).

Our model provides a consistent description of transport in high-mobility polymer FETs as well as polycrystalline oligomer FETs. For the latter, recent results, which contradict earlier experiments (*20*), have shown that as the crystalline order of the organic layers improves, the mobility becomes independent of temperature (*12*, *21*). For the much less perfectly ordered P3HT, an increase in the crystallite grain size and a reduction of the density of localized states will result in lower threshold voltages, reduced activation energies, and possibly even higher mobilities.

The high-mobility polymer FET demonstrated here with a high ON-OFF ratio and good postprocessing robustness approaches the requirements for all-polymer, multilayer electronic and optoelectronic integrated circuits. With some further improvement of FET performance, polymer logic circuits and active matrix addressing in all-polymer LED displays might be feasible.

Note added in proof: Since submission of the final version of the manuscript, we have become aware that an organic LED driven by a polymer FET has independently been demonstrated (*22*).

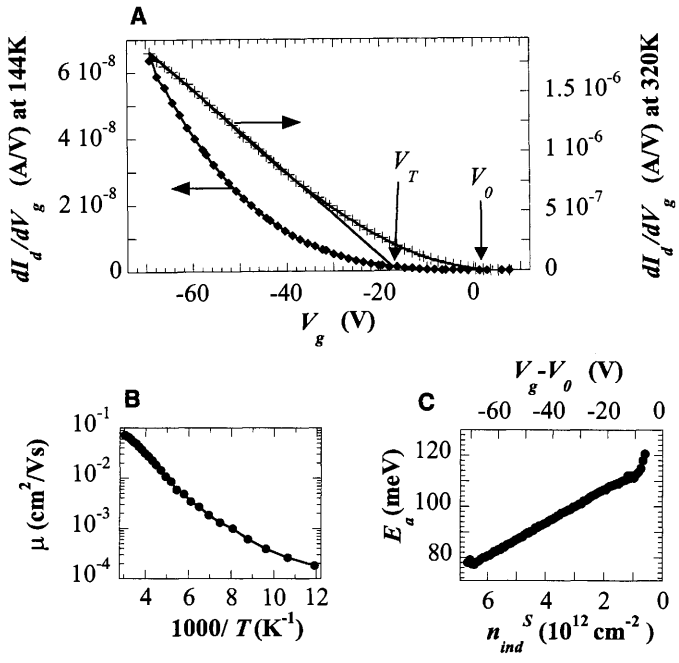

Fig. 4. (**A**) Transconductance dI_d/dV_g in the saturation regime (L = 75 μm, W = 1500 μm, V_{sd} = −70 V) at 320 K (crosses) and 144 K (squares). (**B**) Field-effect mobility at $n^S_{ind} = 6 \times 10^{12}$ cm^{-2} as a function of temperature between 330 and 84 K. (**C**) Activation energy E_a of the mobility extracted between 300 and 160 K as a function of $n^S_{ind} \approx C_i/e(V_g - V_0)$.

REFERENCES AND NOTES

1. N. Tessler, N. T. Harrison, R. H. Friend, *Adv. Mater.* **10**, 64 (1998).
2. See, for example, the World Wide Web site of Cambridge Display Technology (www.cdtltd.co.uk).
3. A. R. Brown, A. Pomp, C. M. Hart, D. M. de Leeuw, *Science* **270**, 972 (1995).
4. J. H. Burroughes, C. A. Jones, R. H. Friend, *Nature* **335**, 137 (1988).
5. A. R. Brown, C. P. Jarrett, D. M. de Leeuw, M. Matters, *Synth. Met.* **88**, 37 (1997).
6. C. C. Wu *et al.*, *IEEE Electron Device Lett.* **18**, 609 (1997).
7. Z. Bao, A. Dodabalapur, A. J. Lovinger, *Appl. Phys. Lett.* **69**, 4108 (1996).
8. The regioregular P3HT with HT coupling >98.5% was obtained commercially from Aldrich Ltd., Dorset, UK. The synthesis route is described in T.-A. Chen, X. Wu, R. D. Rieke, *J. Am. Chem. Soc.* **117**, 233 (1995).
9. C. W. Tang and B. C. Hseih, U.S. Patent 5 550 066 (1996).
10. D. Braun and A. J. Heeger, *Appl. Phys. Lett.* **58**, 1982 (1991); for a review, see N. C. Greenham and R. H. Friend, in *Solid State Physics*, vol. 49, H. Ehrenreich and F. Spaepen, Eds. (Academic Press, San Diego, CA, 1995), pp. 1–149.
11. G. Horowitz, F. Garnier, A. Yassar, R. Hajlaoui, F. Kouki, *Adv. Mater.* **8**, 52 (1996).
12. S. F. Nelson, Y. Y. Lin, D. J. Gundlach, T. N. Jackson, *Appl. Phys. Lett.* **72**, 1854 (1998).
13. H. Sirringhaus, N. Tessler, R. H. Friend, unpublished data.
14. Only at the source-drain contacts do the carriers

have to travel normal to the layer structure. The film thickness must be sufficiently small to keep the contact resistance low (Fig. 3B).
15. M. Shur, M. Hack, J. G. Shaw, *J. Appl. Phys.* **66**, 3371 (1989); M. Shur and M. Hack, *ibid.* **55**, 3831 (1984).
16. G. Horowitz and P. Delannoy, *ibid.* **70**, 469 (1991).
17. K. D. Mackenzie, A. J. Snell, I. French, P. G. Le Comber, W. E. Spear, *Appl. Phys. A* **31**, 87 (1983); A. C. Hourd and W. E. Spear, *Philos. Mag. B* **51**, L13 (1984).
18. This is not the result of an increase of V_0 (Fig. 3A) shifting only slightly from $V_0 \approx 3$ V at 320 K to $V_0 \approx -2.5$ V at 144 K.
19. It was assumed that V_0, which is read directly from the transfer characteristics, can be taken as a rough estimate for V_{FB}, that is, $n^S_{ind} \approx C_i/e(V_g - V_0)$.
20. L. Torsi, A. Dodabalapur, L. J. Rothberg, A. W. P. Fung, H. E. Katz, *Science* **272**, 1462 (1996).
21. ———, *Phys. Rev. B* **57**, 2271 (1998).
22. A. Dodabalapur *et al.*, *Appl. Phys. Lett.*, in press.
23. We thank B. K. Papworth for the photograph, P. Brown and M. Matters for discussions, I. Musa for growing the SiO_2 gate oxide, and Cambridge Display Technology for the MEH-PPV polymer. Supported by the European Commission (ESPRIT 24793–Frequent) and the Engineering and Physical Sciences Research Council.

16 March 1998; accepted 23 April 1998

Carbon Nanotube Quantum Resistors

Stefan Frank, Philippe Poncharal, Z. L. Wang, Walt A. de Heer*

The conductance of multiwalled carbon nanotubes (MWNTs) was found to be quantized. The experimental method involved measuring the conductance of nanotubes by replacing the tip of a scanning probe microscope with a nanotube fiber, which could be lowered into a liquid metal to establish a gentle electrical contact with a nanotube at the tip of the fiber. The conductance of arc-produced MWNTs is one unit of the conductance quantum $G_0 = 2e^2/h = (12.9 \text{ kilohms})^{-1}$. The nanotubes conduct current ballistically and do not dissipate heat. The nanotubes, which are typically 15 nanometers wide and 4 micrometers long, are several orders of magnitude greater in size and stability than other typical room-temperature quantum conductors. Extremely high stable current densities, $J > 10^7$ amperes per square centimeter, have been attained.

The intriguing possibility that nanoscopic graphitic structures may someday be used as electronic elements has been reinforced by predictions (*1*) as well as recent demonstrations (*2–4*) of their device properties. However, not much is known about the electronic transport in nanotubes. Theory predicts that the electrons flow ballistically through them and that the conductance (the inverse of the resistance) is quantized (*5–7*), but neither effect has been observed previously (*3, 4, 8–13*).

Quantized conductance results from the electronic wave guide properties of extremely fine wires and constrictions [see, for example, (*13–20*)]. When the length of the conductor is smaller than the electronic mean free path, then the electronic transport is ballistic, in which case each transverse wave guide mode or conducting channel contributes G_0 to the total conductance. Calculations indicate that conducting single-shell nanotubes have two conductance channels (*5–7*). This predicts that the conductance of a single-wall nanotube (SWNT) is $2G_0$ independent of diameter and length.

Another important aspect of ballistic transport is that no energy is dissipated in the conductor (*20*). Instead, the Joule heat is dissipated in the electrical leads, which connect the ballistic conductor to the macroscopic elements of the circuit. The nondissipative property survives if elastic scattering occurs, for example, from impurities and defects. However, elastic scattering affects the transmission coefficients and thereby reduces the conductance (*20–22*), which then is no longer precisely quantized [see (*19*)].

Until recently, conductance quantization had only been observed in two-dimensional electron gases at ultralow temperatures (*15*). Room-temperature quantized conductance has now also been observed in metallic wires, which usually are at most a few nanometers long and a fraction of a nanometer wide (*16–19*). Although conductance quantization requires ballistic transport (*20–22*), we were able to demonstrate both properties independently.

In our experimental scheme we used arc-produced multiwalled carbon nanotubes (MWNTs) (*23–26*). The nanotubes were typically very straight with lengths of 1 to 10 μm (*24, 25*) (Fig. 1). High-resolution transmission electron microscopy (HRTEM) showed that their diameters ranged from 5 to 25 nm, with inner cavities from 1 to 4 nm; they typically had about 15 layers (*25*). The nanotubes were embedded in fibers that occur in the soft material inside the hard-shelled deposit of the arc (*24, 25*). These fibers are very fine and compact (nominally 50 μm in diameter at the tips and 1 mm long) and are composed of nanotubes and graphitic particles; TEM revealed that usually several particularly long (>3 μm) nanotubes protrude from the tip of the fiber. The protruding nanotubes are usually bundled with others of different lengths, hence only one nanotube is at the extreme end. An example is shown in Fig. 1. The nanotube fiber was attached to a gold wire with colloidal silver paint, and the resulting nanotube contact was installed in place of the tip of a scanning probe microscope (SPM) (*27*) so that the nanotube contact could be raised and lowered using the SPM controls. A heatable copper reservoir containing mercury (or other low–melting temperature metal) was placed below the nanotube contact. The liquid metal was used as the second contact to the nanotubes and allows a gentle and reproducible contact with the nanotubes to be made (mercury does not wet the nanotubes). Moreover, TEM revealed that before the nanotubes are dipped in the liquid metal, they are covered with fine graphitic particles. Dipping them had a cleansing effect, and afterward the protruding

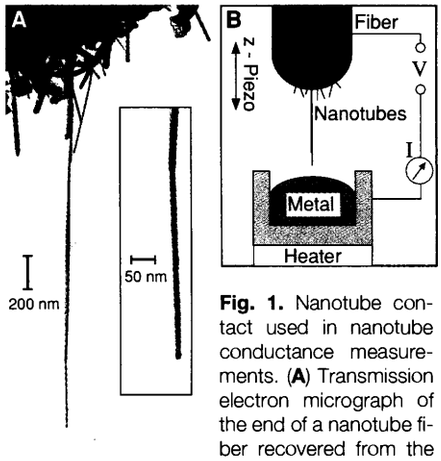

Fig. 1. Nanotube contact used in nanotube conductance measurements. (**A**) Transmission electron micrograph of the end of a nanotube fiber recovered from the nanotube arc deposit. The fibers consist of carbon nanotubes and small graphitic particles. The fiber shown here is ~1 mm long and 0.05 mm at the tip, from which protrude several long and straight nanotubes. The nanotubes are very clean after they have been dipped in liquid metal (like the one shown), in contrast to the virgin tips on which many small graphitic particles are seen. The long nanotube is 2.2 μm long and 14 nm wide. The inset shows the end of the longest tube under higher magnification; it is bundled together with another one that terminates 400 nm before the first one. (**B**) Schematic diagram of the experimental setup. The nanotube contact is lowered under SPM control to a liquid metal surface. After contact is established, the current *I* is measured as the fiber is moved into the liquid metal, so that the conductance can be determined as a function of the position of the nanotube contact.

S. Frank, P. Poncharal, W. A. de Heer, School of Physics, Georgia Institute of Technology, Atlanta GA 30332, USA. Z. L. Wang, School of Materials Science and Engineering, Georgia Institute of Technology, Atlanta GA 30332, USA.

*To whom correspondence should be addressed.